A Novel Blind Deconvolution Scheme for Image Restoration Using Recursive Filtering

Deepa Kundur, *Student Member, IEEE*, and Dimitrios Hatzinakos, *Member, IEEE*

***Abstract*—In this paper, we present a novel blind deconvolution technique for the restoration of linearly degraded images without explicit knowledge of either the original image or the point spread function. The technique applies to situations in which the scene consists of a finite support object against a uniformly black, grey, or white background. This occurs in certain types of astronomical imaging, medical imaging, and one-dimensional (1-D) gamma ray spectra processing, among others. The only information required are the nonnegativity of the true image and the support size of the original object. The restoration procedure involves recursive filtering of the blurred image to minimize a convex cost function. We prove convexity of the cost function, establish sufficient conditions to guarantee a unique solution, and examine the performance of the technique in the presence of noise. The new approach is experimentally shown to be more reliable and to have faster convergence than existing nonparametric finite support blind deconvolution methods. For situations in which the exact object support is unknown, we propose a novel support-finding algorithm.**

I. Introduction

IN MANY imaging applications, the degradation of the true image can be modeled as

$$g(x,y) = h(x,y) * f(x,y) + n(x,y) \tag{1}$$

where

(x,y)	discrete pixel coordinates of the image frame;
$g(x,y)$	blurred image;
$f(x,y)$	true image;
$h(x,y)$	point spread function (PSF);
$n(x,y)$	additive noise;
$*$	discrete two-dimensional (2-D) linear convolution operator.

In this model, the observed image $g(x,y)$, true image $f(x,y)$, and noise $n(x,y)$ are coupled linearly; therefore, the problem of recovering $f(x,y)$ from $g(x,y)$ is referred to as the *linear image restoration problem*. The existing linear image restoration algorithms assume that the PSF is known *a priori* and attempt to invert it and reduce noise by using varying amounts of information about the PSF, true image, and noise statistics [1].

In many situations, however, the PSF is unknown, and little can be assumed about the original image. Therefore, the majority of existing linear image restoration techniques are not applicable for solving this type of problem. The process of simultaneously estimating the PSF (or its inverse) and restoring an unknown image using partial or no information about the imaging system is known as *blind image restoration*. For the linear degradation model of (1), where the noise term $n(x,y)$ is neglected, it is specifically referred to as *blind deconvolution*.

There exist several motivating factors for the use of blind deconvolution in image processing applications. In many situations, it is difficult to accurately measure the degradation using calibration or on-line identification techniques; in addition, it is costly, dangerous, or physically impossible to obtain *a priori* information about the scene to be imaged. For example, in remote sensing and space imaging, fluctuations in the PSF are difficult to characterize as a random process, and there is difficulty in statistically modeling the original image [2]. In addition, the use of adaptive optics systems are often too expensive for some observation facilities, and the potential for phase error exists with cheaper partially compensating systems. Thus, post processing such as blind deconvolution still may be required [3]. It is clear that the development of a practical blind deconvolution scheme for images would benefit many imaging facilities.

In practice, some *a priori* information is required to restore the image successfully. The partial information available is specific to each imaging application; therefore, many diverse techniques for blind deconvolution of images have been proposed. The challenge is to design a method that exhibits the most appropriate compromise among computational complexity, reliability, robustness to noise, and portability for a given application. We provide a brief outline of existing techniques in Section II.

The first contribution of this paper is the development of a novel blind deconvolution technique for the restoration of linearly degraded images. Explicit knowledge of either the original image or point spread function is not required. The proposed technique [4] is relevant to applications in which an object of finite extent is imaged against a uniformly black, grey, or white background. The edges of the object are assumed to be completely or almost completely included within the observed frame. This often occurs in some types of astronomical imaging, medical imaging, among others. The only information required for restoration is the nonnegativity of the true image and support size of the original object. The restoration procedure involves recursive filtering of the blurred image to minimize a convex cost function. The advantage

Manuscript received June 28, 1995; revised August 12, 1997. This work was supported by the Natural Sciences and Engineering Research Council (NSERC) of Canada. The associate editor coordinating the review of this paper and approving it for publication was Dr. Nurgun Erdol.

The authors are with the Department of Electrical and Computer Engineering, University of Toronto, Toronto, Ont., Canada M5S 3G4.

Publisher Item Identifier S 1053-587X(98)01345-2.

of the proposed technique over existing methods is that convergence to the feasible set of solutions is guaranteed. We discuss the specific problem we address and introduce the novel blind deconvolution technique in Sections III and IV, respectively. A proof of the convexity of the associated cost function and a discussion of the uniqueness of the solution are given in Section IV-B and Appendixes A and B. We derive analytic expressions for the performance of the technique in the presence of noise in Appendix C and propose methods of compensating for the undesirable effects of additive noise in Section IV-C.

The second contribution is the design of a novel support-finding algorithm for situations in which the size of the original object is unknown. The algorithm is based on the principle of cross-validation. We provide a discussion of the technique in Section V.

The third contribution of this paper is a comparative study of the performance of the proposed technique with other methods belonging to the class of nonparametric, finite support blind deconvolution methods. The proposed technique is shown to produce more reliable results and to converge faster than the other methods for complex grey-scale images. In addition, it is more robust to overestimation of the support size. Section VI presents simulation results showing the quality of restored images for each method. Even though this paper deals in particular with 2-D signals, this work applies equally for one-dimensional (1-D) applications such as gamma ray spectra processing.

II. Existing Blind Image Deconvolution Techniques

Most of the available blind deconvolution methods for images apply to the restoration of grey-scale images. They are grouped into classes based on their assumptions about the true image and PSF. Early techniques [5] attempt to identify the PSF from the degraded image characteristics before restoration of the image. A parametric model for the PSF is assumed with spectral nulls at locations dependent on the specific parameter values; these parameter values are estimated using the spectral nulls of the degraded image. Although the method has low computational complexity, it is sensitive to noise and is limited to situations in which the PSF contains spectral nulls.

Lane and Bates have shown that any degraded image g formed by convolving several individual components $f_1, f_2, \cdots, f_n$ having compact support is automatically deconvolvable using zero sheet separation techniques provided its dimension is greater than one [6]. The major drawbacks of the algorithm are its sensitivity to noise and its high computational complexity.

In ARMA parameter estimation methods, the true image is modeled statistically as a 2-D autoregressive (AR) process and the PSF as a 2-D linear system with finite impulse response; therefore, the blurred image is represented by a 2-D ARMA process. Several approaches have been proposed to estimate the ARMA parameters [7], [8]. The techniques are reasonably robust to noise but can suffer from ill-convergence and phase ambiguity and, for practical success, require that a parametric form of the blur be available.

A similar method models the true image and additive noise as multivariate Gaussian processes [9], [10]. Maximum-likelihood (ML) estimates of the PSF parameters and of the covariance matrix parameters for the true image and the noise are computed to perform blind deconvolution. Due to the high degree of nonlinearity, the necessary optimization is difficult and is conducted using the expectation-maximization (EM) algorithm. As only second-order statistics are used in the estimation process, the algorithm applies to the identification of nonminimum phase PSF's. The main advantages of the technique are that a parametric form of the PSF and its support size are not required for restoration and that the algorithm has low computational complexity. The main obstacle is that the EM algorithm may converge to a local optima during the maximization process.

ML EM-based techniques are also used for the blind deconvolution of light microscopic images [11]–[13]. The approach takes into account the statistical nature of the quantum photon emissions. Nonnegativity and bandlimit constraints among others are imposed on the image and/or PSF. The main advantage of the approach is the inherent noise suppression for oversampled images. The major limitation is its computational speed.

Another class of blind deconvolution techniques applies to the restoration of texture images [15]. The techniques are based on the minimization of a given cost function, which accounts for the probabilistic nature of the true image by making use of its higher order statistics (HOS). These methods allow the identification of nonminimum phase PSF's but require that the true image be represented by a known non-Gaussian probability distribution.

Multichannel techniques are proposed for situations in which differently blurred versions of the same image are available for processing. The most successful methods of this class are the *cepstrum based high-order statistics algorithms* [16], [17]. The approach combines partial, higher order cepstral information from two differently blurred frames to estimate the true image. The major limitation is that the method is computationally intensive for 2-D signals and is implemented only for 1-D blurs.

The final class of methods is called nonparametric finite support restoration techniques. The true image is assumed to be positive and to be comprised of an object with known finite *support* against a uniformly black, grey, or white background. The support is defined as the smallest rectangle within which the unblurred object is completely encompassed. Several approaches fall under this class [18]–[22], including the proposed blind deconvolution method. Existing techniques suffer from poor convergence properties and lack reliability. The new approach is shown to produce more accurate results and to have faster convergence than existing nonparametric finite support blind deconvolution methods.

A more detailed review of existing blind image deconvolution techniques can be found in [23].

III. Problem Formulation

The objective of blind image deconvolution is to construct a reliable estimate of the imaged scene from a blurred version.

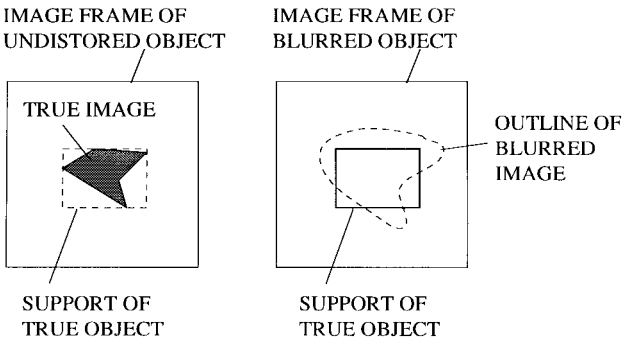

Fig. 1. Example of a finite support image. The support of the true image is different from the support of the blurred image.

This task is achieved by using partial information about the imaging process as a *reference* to deconvolve the true image and PSF from the blurred image.

In this paper, we make the following assumptions about the imaging process, the true image, and the PSF.

1) The degradation is described by the linear model of (1).
2) Imaging is performed such that the object is entirely encompassed by the observed frame.
3) The background of the image is uniformly grey, black, or white.
4) The true image is nonnegative, and its support is known *a priori*; the support is defined to be the smallest rectangle encompassing the object of interest (Fig. 1 illustrates the region of support).
5) The true image and PSF are *irreducible*; the term irreducible refers to a signal that cannot be expressed as the convolution of two or more component images of finite support on the understanding that the delta function is not a component image.
6) The inverse of the PSF exists, and both the PSF and its inverse are absolutely summable (that is, $\Sigma_{x=-\infty}^{\infty} \Sigma_{y=-\infty}^{\infty}|h(x,y)| < \infty$ and $\Sigma_{x=-\infty}^{\infty} \Sigma_{y=-\infty}^{\infty}|h^{-1}(x,y)| < \infty$).
7) In the situation where the background of the image is black, the sum of all PSF pixels is assumed to be positive, which occurs in almost all image processing applications.

Note that Assumption 6 is somewhat restrictive. For example, in microscopy applications, the PSF has a cone-shaped spectral null. This, however, implies that its inverse is not absolutely summable. Hence, the proposed algorithm cannot be used for such applications. As we explain in Section IV, Assumption 7 is required to avoid the trivial all-zero solution to the problem, which can occur in certain situations.

No other constraints are imposed on the PSF. If the actual support of the true image is unknown, we use a novel support-finding algorithm, which is described in Section V, to determine the extent of the object. The other algorithms of this class require the PSF to be nonnegative and have known support.

Constraints of nonnegativity and support have been used in nonblind restoration problems to improve the resolution of gamma-ray spectra [24]. Evidence exists that nonnegativity and support information can extrapolate the high-frequency components lost when the distortion is bandlimiting [25]; therefore, such constraints hold promise in blind image restoration.

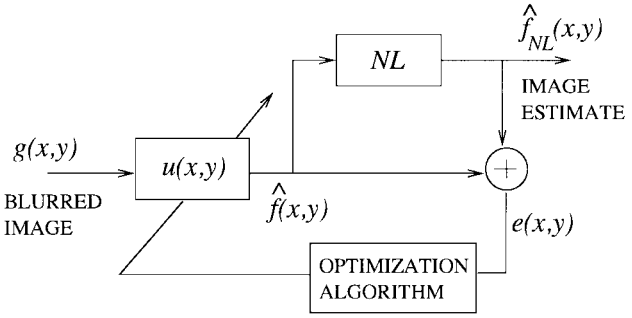

Fig. 2. Proposed blind image deconvolution method.

The problem requires computing an image estimate $\hat{f}(x,y)$, given $g(x,y)$, by minimizing an error metric that incorporates knowledge of the support and nonnegativity of the true image. A solution that globally minimizes the error metric is termed a *feasible* solution. The objective is to obtain the true image up to a positive constant multiplier and displacement. That is

$$\hat{f}(x,y) = Kf(x - D_x, y - D_y). \tag{2}$$

IV. The Nonnegativity and Support Constraints Recursive Invese Filtering (NAS-RIF) Algorithm

A. General Overview

The proposed method is referred to as the nonnegativity and support constraints recursive inverse filtering (NAS-RIF) algorithm. The blurred image $g(x,y)$ is input to a 2-D variable coefficient FIR filter $u(x,y)$ whose output represents an estimate of the true image denoted $\hat{f}(x,y)$. This estimate is passed through a nonlinear constraint process that uses a nonexpansive mapping to project the estimated image into the space representing the known characteristics of the true image. The difference between the projected image $\hat{f}_{NL}(x,y)$ and $\hat{f}(x,y)$ is used as an error signal to update the coefficients of filter $u(x,y)$. Fig. 2 gives an overview of the method.

For the NAS-RIF algorithm, the image is assumed to be nonnegative with known support; therefore, $\hat{f}_{NL}(x,y)$ represents the projection of the estimated image onto the set of images that are nonnegative with given finite support. This requires replacing the negative pixel values within the region of support with zero and pixel values outside the region of support with the background grey-level value L_B. The cost function used in the restoration procedure is defined as

$$J = \sum_{\forall(x,y)} [\hat{f}_{NL}(x,y) - \hat{f}(x,y)]^2 \tag{3}$$

where

$$\hat{f}_{NL}(x,y) = \begin{cases} \hat{f}(x,y) & \text{if } \hat{f}(x,y) \geq 0 \text{ and } (x,y) \in D_{\text{sup}} \\ 0 & \text{if } \hat{f}(x,y) < 0 \text{ and } (x,y) \in D_{\text{sup}} \\ L_B & \text{if } (x,y) \in \overline{D_{\text{sup}}}. \end{cases} \tag{4}$$

Using (4), (3) reduces to

$$J = \sum_{(x,y)\in D_{\text{sup}}} \hat{f}^2(x,y)\left[\frac{1-\text{sgn}(\hat{f}(x,y))}{2}\right] + \sum_{(x,y)\in \overline{D_{\text{sup}}}} [\hat{f}(x,y) - L_B]^2 \quad (5)$$

where the definition for sgn$(\cdot)$

$$\text{sgn}(f) \triangleq \begin{cases} 1, & \text{if } f \geq 0 \\ -1, & \text{if } f < 0 \end{cases} \quad (6)$$

is used, $\hat{f}(x,y) = g(x,y) * u(x,y)$, D_{sup} is the set of all pixels inside the region of support, and $\overline{D_{\text{sup}}}$ is the set of all pixels outside the region of support. As we can see, for situations in which the background is black (i.e., $L_B = 0$), the parameter set $u(x,y) = 0$ for all (x,y) globally minimizes J. This results in a restored image $\hat{f}(x,y) = 0$ for all (x,y), which is the all-black solution. To avoid this trivial solution, we make use of Assumption 7 of Section III, which states that the sum of all the PSF coefficients is positive, i.e.,

$$\sum_{\forall(x,y)} h(x,y) = S_h > 0. \quad (7)$$

Using the fact that the 2-D discrete-time Fourier transform of $h(x,y)$ at $\omega = 0$ is given by

$$H(0) = \sum_{\forall(x,y)} h(x,y) \quad (8)$$

we can deduce that

$$H(0) = S_h > 0. \quad (9)$$

Taking the reciprocal of both sides and letting $h_{\text{inv}}(x,y)$ and $H_{\text{inv}}(\omega)$ be the spatial and Fourier transform functions of the ideal inverse of $h(x,y)$, respectively, we see that

$$H_{\text{inv}}(0) = \frac{1}{H(0)} = \frac{1}{S_h} \quad (10)$$

or, effectively

$$\sum_{\forall(x,y)} h_{\text{inv}}(x,y) = \frac{1}{S_h} > 0. \quad (11)$$

Thus, we can deduce that the sum of the pixels of the inverse PSF is also positive. We can use this fact to constrain the parameters $\{u(x,y)\}$ from the trivial all-zero solution.

Since our goal is to obtain a positive scaled version of the ideal image $f(x,y)$, we can constrain the sum of all the filter coefficients $u(x,y)$ to be any positive constant to meet this objective. In this paper, we choose $S_h = 1$ so that we have the following constraint on our FIR filter coefficients:

$$\sum_{\forall(x,y)} u(x,y) = 1. \quad (12)$$

In the implementation of the NAS-RIF algorithm, we use the iterative conjugate gradient minimization routine. One option for constraining the parameters to fulfill (12) is to normalize u at every iteration. Research, however, indicates that this method of constraint is computationally inefficient for use with the conjugate gradient minimization routine [26], [27]. Thus, we use a penalty method and add a third term to the cost function. The overall function is represented by

$$J = \sum_{(x,y)\in D_{sup}} \hat{f}^2(x,y)\left[\frac{1-\text{sgn}(\hat{f}(x,y))}{2}\right] + \sum_{(x,y)\in \overline{D_{\text{sup}}}} [\hat{f}(x,y) - L_B]^2 + \gamma\left[\sum_{\forall(x,y)} u(x,y) - 1\right]^2. \quad (13)$$

The cost function consists of three components. The first penalizes the negative pixels of the image estimate inside the region of support, and the second penalizes the pixels of the image estimate outside the region of support that are not equal to the background color. The first component prevents the pixels of the intermediate restorations from becoming highly negative and can have the effect of increasing convergence of the NAS-RIF algorithm. It also has the effect of reducing noise amplification when additive noise is present in the degraded image. The nonnegative real variable γ in the third component of (13) is nonzero only when L_B is zero, i.e., the background color is black. This third component, as discussed, is used to constrain the FIR filter coefficients $u(x,y)$ away from the trivial all-zero global minimum.

It is shown in Appendix A that the cost function of (13) is convex with respect to the FIR filter coefficients $\{u(x,y)\}$; therefore, convergence of the algorithm to the global minimum is possible using a variety of numerical optimization methods. The conjugate gradient minimization routine is used for the minimization of J because its speed of convergence is, in general, much faster than other descent methods. One of the advantages of this routine is that convergence in a finite number of iterations is guaranteed when a quadratic cost function is used and exact arithmetic is assumed. Even for nonquadratic costs, the method shows considerably increased convergence speed relative to the steepest descent method [27]. The algorithm is based on the premise that information about the curvature of J at each iteration can accelerate the minimization process. The NAS-RIF algorithm is summarized in Table I.

B. Convergence Properties

This section addresses the convergence and uniqueness properties of the NAS-RIF algorithm. The major advantage of the algorithm is that it entails the minimization of a convex cost function. All other existing nonparametric finite support restoration techniques involve the minimization of nonconvex costs and, practically, do not guarantee convergence to the global solution. In Appendix A, we provide a formal proof of convexity of the proposed cost function of (13).

Convexity of the cost function implies that J does not contain local optima. However, it does not necessarily imply that the solution to the problem is unique. It is critical to differentiate between the uniqueness of the global minimum of the cost function J and the uniqueness associated with the

TABLE I
SUMMARY OF THE NAS-RIF ALGORITHM

- Definitions:
  - $\boldsymbol{u}_k$ is the vector of filter coefficients $u(x,y)$ of dimension $N_{xu} \times N_{yu}$ in lexicographical order at the kth iteration.
  - $u_k(x,y)$ is the filter $u(x,y)$ at kth iteration.
  - $J(\boldsymbol{u}_k)$ is the cost function of Equation (13) at parameter setting $\boldsymbol{u}_k$.
  - $\nabla J(\boldsymbol{u}_k)$ is the $N_{xu}N_{yu} \times 1$ gradient vector of J at $\boldsymbol{u}_k$.
  - $[\boldsymbol{M}]_{x,y}$ denotes the xth row and yth column of matrix $\boldsymbol{M}$
  - $< \cdot, \cdot >$ represents the inner product operator.
  - $\| \cdot \|$ is the Eucledian norm.
  - D_{sup} is the set of pixels inside the region of support.
  - $\overline{D_{sup}}$ is the set of pixels outside the region of support.
- Set initial conditions ($k = 0$):

  FIR filter: $\boldsymbol{u}_k^T = [u_k(1,1), \ldots, u_k(N_{xu}+1)/2, (N_{yu}+1)/2, \ldots, u_k(N_{xu}, N_{yu})] = [0, \ldots, 1, \ldots, 0]$
  tolerance: $\delta > 0$ is set.

- At iteration (k): $k = 0, 1, 2, \ldots$

  1) If $J(\boldsymbol{u}_k) \leq \delta$, stop.

  2) Calculate the gradient vector of J,

  a) $f_k(x,y) = u_k(x,y) * g(x,y)$

  b) $[\nabla J(\boldsymbol{u}_k)]_{j+(i-1)N_{xu},1} = \frac{\partial J(\boldsymbol{u}_k)}{\partial u(i,j)}$
  $= 2\sum_{(x,y)\in D_{sup}} \hat{f}_k(x,y)\mathrm{cl}(\hat{f}_k(x,y))g(x-i+1, y-j+1) + 2\sum_{(x,y)\in \overline{D_{sup}}}[\hat{f}_k(x,y) - L_B]g(x - i + 1, y - j + 1) + 2\gamma\left[\sum_{\forall(x,y)} u(x,y) - 1\right]$ where $\mathrm{cl}(\cdot)$ is defined as in Equation (43).

  3) If $k = 0$, $\boldsymbol{d}_k = -\nabla J(\boldsymbol{u}_k)$.
  Otherwise,

  a) $\beta_{k-1} = \frac{<\nabla J(u_k) - \nabla J(u_{k-1}), \nabla J(u_k)>}{\|\nabla J(u_{k-1})\|^2}$

  b) $\boldsymbol{d}_k = -\nabla J(\boldsymbol{u}_k) + \beta_{k-1}\boldsymbol{d}_{k-1}$

  4) Perform a line minimization such as `dlinmin.c` in [39], to find t_k such that

  $$J(\boldsymbol{u}_k + t_k\boldsymbol{d}_k) \leq J(\boldsymbol{u}_k + t\boldsymbol{d}_k) \quad \text{for } t \in \mathbb{R}$$

  5) $\boldsymbol{u}_{k+1} = \boldsymbol{u}_k + t_k\boldsymbol{d}_k$

overall blind deconvolution problem. To avoid confusion, we will attempt to contrast these related topics.

We may show intuitively that the solution to the blind deconvolution problem is, in general, not unique. For example, if $f(x,y)$ is irreducible (i.e., $f(x,y) = f_1(x,y) * f_2(x,y)$ where $f_1(x,y), f_2(x,y) \neq K\delta(x,y)$), then $g(x,y)$ can be represented as

$$\begin{aligned} g(x,y) &= f(x,y) * h(x,y) \\ &= f_1(x,y) * f_2(x,y) * h(x,y). \end{aligned} \tag{14}$$

Deconvolution of $g(x,y)$ into two components may not necessarily result in $f(x,y)$ and $h(x,y)$; it is possible to obtain $f_1(x,y)$ and $f_2(x,y)*h(x,y)$ or $f_2(x,y)$ and $f_1(x,y)*h(x,y)$. Even if nonnegativity and support information about $f(x,y)$ is known, it is possible to have ambiguous solutions because $f_1(x,y)$ and $f_2(x,y)$ can both be nonnegative and are zero outside the support of $f(x,y)$. This is a limitation of blind deconvolution. Because little information is available about the imaging system, ambiguous solutions may result. The assumption that the true image $f(x,y)$ is irreducible eliminates many of these situations.

The previous discussion also pertains to the NAS-RIF algorithm for noiseless conditions and assuming an infinite extent inverse filter. If $f_2(x,y) * h(x,y)$ is invertible, then it can be shown that $u_1(x,y) = [f_2(x,y) * h(x,y)]^{-1}$ [which results in an image estimate $\hat{f}(x,y) = f_1(x,y)$] will globally minimize J. Similarly, if $f_1(x,y) * h(x,y)$ is invertible, then $u_2(x,y) = [f_1(x,y) * h(x,y)]^{-1}$ [which results in $\hat{f}(x,y) = f_2(x,y)$] will also globally minimize J. In fact, it can be shown that $J(h^{-1}) = J(u_1) = J(u_2) = 0$. Thus, minimizing J may result in one of several solutions, most of which are physically meaningless to the problem. The irreducibility assumption can successfully eliminate this problem.

In practice, however, $u(x,y)$ is of finite extent and must approximate $h^{-1}(x,y)$ closely enough to produce an image estimate "highly similar" to the true image. Even if the

irreducibility of $f(x,y)$ is imposed, the minimization of J with respect to the finite extent filter $u(x,y)$ may not result in a unique solution. The uniqueness of $u(x,y)$ in this situation is related to the unimodality of J with respect to u.

A distinction between convexity and *strict-sense* convexity is important. A convex function implies that the function does not contain any local optima. However, there can exist a set of points, all of which globally minimize the function. In contrast, strict-sense convexity implies that the cost function is unimodal, that is, it has a unique global minimum. In Appendix A, we prove that J is convex. Appendix B shows that a sufficient condition for J to be unimodal (i.e., strictly convex) is that the pixels of the blurred image $g(x,y)$ must form $N_{xu}N_{yu}$ linearly independent vectors g_{xy}, which are defined as

$$g_{xy}^T = [g(x,y)\ g(x,y-1)\ g(x,y-2) \cdots g(x-N_{xu}+1, y-N_{yu}+1)] \tag{15}$$

where $(x,y) \in \overline{D_{\text{sup}}}$, and $N_{xu} \times N_{yu}$ are the dimensions of the FIR filter $u(x,y)$. Experience shows that for practical images, this condition almost always holds, and the solution to the proposed algorithm for finite coefficients is almost always unique.

C. Effects of Noise

The effects of noise for the classical linear image restoration problem have been studied [29]. The analysis is somewhat more difficult for blind deconvolution as little information is known about the imaging process.

1) Ill-Posed Nature of the Blind Deconvolution Problem: Deconvolution is an ill-posed problem because small perturbations of the given data produce large deviations in the resulting solution. The particular process of inverse filtering attempts to restore the image by direct-inversion of the PSF; therefore, the problem is ill posed due to the presence of additive noise. This follows because the direct inverse of the PSF transfer function often has a large magnitude at high frequencies; therefore, excessive amplification of the noise at these frequencies results.

Although convexity is preserved in the presence of noise for the proposed NAS-RIF algorithm, $\nabla^2 J$ may lose rank, and thus, J may lose unimodality due to the perturbations of $g(x,y)$. The problem is, therefore, formally classified as ill posed [30]. We discuss regularization methods to combat the ill-posed nature of the problem in Section IV-C3.

2) Bias Introduced by the Presence of Additive Noise: The analysis of the effect of noise on the cost function provides insight into the behavior of the NAS-RIF algorithm in practical situations. Because the cost function J is nonlinear, its global minimum in the presence of noise u^*_{noise} is difficult to characterize in terms of its minimum in the noiseless case u^*. However, if we consider the continuity of J with respect to u, we see that the value of the cost function in noisy conditions at the ideal parameter setting u^* is an effective indicator of the degree of bias introduced in the restored image. We present the results for the case of zero-mean stationary additive white Gaussian noise (AWGN) of variance σ_n^2 in this section. Appendix C provides a detailed analysis. The expected value of the cost at u^* assuming infinite extent coefficients is

$$\begin{aligned} E\{J(u^*(x,y))\} &= \sum_{(x,y)\in D_{\text{sup}}} (f^2(x,y)+\sigma^2)\left(1 - Q\left(\frac{-f(x,y)}{\sqrt{2}\sigma}\right)\right) \\ &\quad - \sum_{(x,y)\in D_{\text{sup}}} \sigma \frac{f(x,y)}{\sqrt{2\pi}} e^{-f^2(x,y)/2\sigma^2} \\ &\quad + \sigma_n^2 ||D_{\text{sup}}|| \sum_{x_1=-\infty}^{\infty} \sum_{y_1=-\infty}^{\infty} [u^*(x_1,y_1)]^2 \end{aligned} \tag{16}$$

where

$$\sigma^2 = \sigma_n^2 \sum_{x_1=-\infty}^{\infty} \sum_{y_1=-\infty}^{\infty} [u^*(x_1,y_1)]^2. \tag{17}$$

$E\{J(u^*(x,y))\}$ bias term resulting from the presence of noise;
$f(x,y)$ true image;
$u^*(x,y)$ desired equalizer setting in the noiseless situation;
$||\overline{D_{\text{sup}}}||$ number of elements in $\overline{D_{\text{sup}}}$;
$Q(s)$

$$Q(s) \triangleq \frac{1}{\sqrt{2\pi}} \int_s^{\infty} e^{-\xi^2}\, d\xi. \tag{18}$$

The bias is a function of the true image, the variance of the noise σ_n^2, and the energy of the optimal coefficients u^*. The first two terms on the right-hand side of (16) correspond to the bias of the nonnegativity constraint and the last term to the bias of the support constraint. The first two terms imply that the effect of noise is small when the ratio $f(x,y)/\sigma$ is large for all $(x,y) \in D_{\text{sup}}$. Noise has less effect if the image is largely positive because the perturbations have less effect on the restoration with respect to the nonnegativity constraint. The bias related to the support constraint is proportional to the variance of the noise σ_n^2. For a fixed value of σ_n^2, we can see that the noise has less effect on the restoration if the variance of the inverse of the ideal PSF is small, that is, if the inverse PSF is lowpass. Practical PSF's are generally lowpass, and their associated inverses are high pass so that noise amplification is expected in the solution.

3) Compensation for Noise Amplification: To avoid excessive noise amplification, regularization of the problem is usually required. Traditional forms of regularization make use of a smoothness constraint on the true image data [31]; a stabilizing functional can be added to the cost to damp noise amplification. Although this would regularize the problem, it requires knowledge of the smoothness characteristics and/or noise variance. As the problem is blind, these smoothness parameters will have to be estimated through trial and error. Several restorations using different smoothness constraints will have to be generated and evaluated to find the best set of parameters, which will increase computational time.

Regularization can also take the form of terminating an iterative restoration procedure before it converges to the inverse solution. As an iterative restoration process progresses,

the error due to blurring decreases as the error due to noise amplification increases. At some point in the algorithm, this total error reaches a minimum and the procedure should be stopped before convergence. This phenomenon is explained and experimentally investigated in [33]–[36] and has demonstrated the effectiveness of premature algorithm termination in combating noise amplification.

A drawback of the proposed NAS-RIF algorithm is that the convergence point is not necessarily the best estimate of the original image in the presence of noise. The iterative implementation of the inverse filter has the advantage that it can be terminated prior to convergence, resulting in a partially blurred image, which will often exhibit less noise amplification. This would require monitoring image estimate at the output of the nonlinear constraint $f_{NL}(x,y)$ and terminating the process when a "visually optimal" result is achieved. In most situations, some subjective idea of the variance of the image is available. Results of this technique are shown in Section VI.

V. Novel Blind Support-Finding Algorithm

A. Introduction to the Cross-Validation (CV)

Historically, cross-validation (CV) has been used as a criterion for estimating the optimal regularization parameter in smoothing problems, but recently, CV has been applied to image restoration applications [14], [37]. The principle behind CV is straightforward. The data is divided into two sets: an estimation set and a validation set. The estimation set is used to obtain a model or estimate based on a particular parameter value or assumption. The validation set is then used to validate the assumption. In this way, many competing parameter values or assumptions may be tested to find the most appropriate. It is necessary to use as much of the data as possible to obtain a reliable estimate, but it is also desirable to test the estimate on as much of the data that was excluded from the estimation process as possible. CV overcomes this dilemma by allowing all the data to be used for both functions.

B. CV Approach of Determining the Object Support Size

For nonblind image restoration applications [37], the data used for estimation and validation are the given blurred image pixels. An image estimate is produced based on assumptions made about the imaging system. The assumption is validated by "reblurring" (convolving) it using the known PSF and finding the energy of its deviation from the original blurred image pixels excluded from the estimation process.

Because, in blind image restoration, the PSF is unknown, it is impossible to validate an assumption in this way. One method suitable for blind image restoration is to divide the *a priori* information (instead of the blurred image pixels) into estimation and validation sets. We can make use of the fact that we know the image is positive and of finite support. A support region S is assumed, and the pixels outside the assumed support are randomly chosen to be in one of M groups $\{\overline{S}_1,\cdots,\overline{S}_M\}$. All the pixels outside S, which are denoted by $\overline{S}$, are minimized except for those in group l to form a "restored" image estimate $\hat{f}_l(x,y)$ by minimizing the estimation error with respect to $\{u(x,y)\}$ as

$$E(S)=\sum_{(x,y)\in\overline{S}}[\hat{f}(x,y)-L_B]^2 \tag{19}$$

where $\hat{f}(x,y)=u(x,y)*g(x,y)$.

This estimate is validated by calculating the sum of the energies of $(\hat{f}(x,y)-L_B)$ for $(x,y)\in\overline{S}_l$ and the negative pixels within S, which is an objective measure of the authenticity of an assumed support. The validation error is given by

$$V(S)=\frac{1}{M}\sum_{l=1}^{M}\left[\sum_{(x,y)\in\overline{S}_l}[\hat{f}_l(x,y)-L_B]^2+\sum_{(x,y)\in S}\hat{f}_l^2(x,y)\left[\frac{1-\operatorname{sgn}(\hat{f}_l(x,y)}{2}\right]\right]. \tag{20}$$

The support region S^*, which minimizes $V(S)$, is considered to be the optimal support for restoration. In practice, S may be chosen to be any shape, the parameters of which are varied to select the most appropriate support region. For the results presented in this paper, the support is assumed to be rectangular with variable dimensions and fixed orientation.

C. Implementation Issues of the CV Approach

Since the full cross-validation procedure requires M "restorations" to assess a selected support, we suggest implementation of a less computationally demanding approach, which does not substantially sacrifice the performance of the full procedure. The technique is commonly referred to as the *holdout* method.

The validation error may be approximated by computing the error over only a single deleted set of pixels rather than all M sets. This way only a single restoration is required to assess a given support. The expression for the new validation error is

$$V_{HO}(S)=\frac{1}{||\overline{S}_1||}\sum_{(x,y)\in\overline{S}_1}[\hat{f}_1(x,y)-L_B]^2+\frac{1}{||S||}\sum_{(x,y)\in S}\hat{f}_1^2(x,y)\left[\frac{1-\operatorname{sgn}(\hat{f}_1(x,y))}{2}\right] \tag{21}$$

where the deleted set is $\overline{S}_1$.

In general, the CV criterion is difficult to minimize analytically, and numerical techniques must be employed to determine the optimal support parameters. We incorporate a search procedure to find the minimum of the, possibly multimodal, validation error function. Fortunately, simulation results show that the validation error is smooth with respect to support parameters. Any local minima are dominated by large-scale changes in the function. Therefore, the search procedure can initially consist of a selecting points on a widely spaced grid of possible support parameters. The grid is continually made finer to pinpoint the precise location of the minimum. The procedure in algorithmic form for rectangular support is provided in Table II. Results shown in Section VI demonstrate the reliable performance of the procedure.

TABLE II
SUMMARY OF THE BLIND SUPPORT-FINDING ALGORITHM

A) Initialize parameters

- Smallest Test Support: $(N_{xm}, N_{ym}) = (1, 1)$
- Largest Test Support: $(N_{xM}, N_{yM}) = (N_{xg} - 1, N_{yg} - 1)$, where the blurred image is of dimensions $N_{xg} \times N_{yg}$.
- Set Search Interval: $(\Delta L_x, \Delta L_y)$, $1 \leq \Delta L_x \leq N_{xg}/2, 1 \leq \Delta L_y \leq N_{yg}/2$ and $\Delta L_x, \Delta L_y \in \mathbb{Z}$.

B) At iteration (L_x): $L_x = N_{xm}, N_{xm} + \Delta L_x, N_{xm} + \Delta 2L_x, \ldots, N_{xM}$
At iteration (L_y): $L_y = N_{ym}, N_{ym} + \Delta L_y, N_{ym} + \Delta 2L_x, \ldots, N_{yM}$

1) Randomly divide the pixels outside the selected support into M groups $\{\overline{S}_1, \ldots, \overline{S}_M\}$ of equally numbered elements.

2) Based on the assumed support S, "restore" the image by using the NAS-RIF algorithm of Table 1, but using the following definitions for $J(\boldsymbol{u}_k)$ and $\nabla J(\boldsymbol{u}_k)$:

$$J(\boldsymbol{u}_k) = \sum_{(x,y)\in\overline{S}-\overline{S_1}} [\hat{f}_k(x,y) - L_B]^2 \text{ where } \hat{f}_k(x,y) = u_k(x,y) * g(x,y) \tag{55}$$

and

$$[\nabla J(\boldsymbol{u}_k)]_{j+(i-1)N_{xu},1} = 2 \sum_{(x,y)\in\overline{S}-\overline{S_1}} \hat{f}_k(x,y) g(x-i+1, y-j+1) \tag{56}$$

3) Calculate the simplified validation error based on the minimizing parameters $f^*(x,y)$ of step 2.

$$V_{HO}(S) = \frac{1}{\| \overline{S}_1 \|} \sum_{(x,y)\in\overline{S}_1} [\hat{f^*}_1(x,y) - L_B]^2 + \frac{1}{\| S \|} \sum_{(x,y)\in S} \hat{f^*}_1^2(x,y) \left[\frac{1 - \text{sgn}(\hat{f^*}_1(x,y))}{2}\right] \tag{57}$$

C) Let (L_x^*, L_y^*) be the rectangular support dimensions that produces the smallest validation error of Equation (57) from the supports tested so far.

$$\begin{aligned}(N_{xm}, N_{ym}) &= (L_x^* - \Delta L_x, L_y^* - \Delta L_y)\\ (N_{xM}, N_{yM}) &= (L_x^* + \Delta L_x, L_y^* + \Delta L_y)\end{aligned}$$

D) Reduce $(\Delta L_x, \Delta L_y)$. If $(\Delta L_x, \Delta L_y) = (0,0)$, stop. Otherwise, go to Step **B)**.

VI. SIMULATION RESULTS AND COMPARISONS

We provide simulation results of the proposed NAS-RIF algorithm to demonstrate its improved performance over the existing methods. Three popular methods of the class

- iterative blind deconvolution algorithm [18], [19];
- Lane's conjugate gradient method [20];
- McCallum's simulated annealing method [21];

have been implemented for comparison. We briefly describe the techniques here. A more detailed description of the implementation of these algorithms for this study can be found in [4] and [30].

The iterative blind deconvolution method proposed by Ayers and Dainty [18] is, by far, the most popular method in this class of restoration techniques. The basic structure of the algorithm is presented in Fig. 3. The image estimate is denoted by $\hat{f}(x,y)$, the PSF estimate by $\hat{h}(x,y)$, and the linearly degraded image by $g(x,y)$. The capital letters represent fast Fourier transformed versions of the corresponding signals. Subscripts denote the iteration number of the algorithm.

After a random initial guess is made for the image, the algorithm alternates between the image and Fourier domains, enforcing known constraints in each. The constraints are based on information available about the image and PSF.

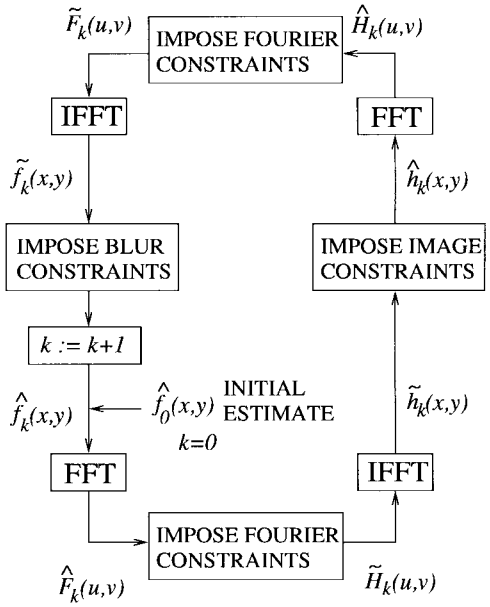

Fig. 3. Iterative blind deconvolution method.

Since the image $f(x,y)$ and PSF $h(x,y)$ are both assumed to be positive with finite known support, the image domain

constraints are imposed by replacing negative-valued pixels within the region of support and nonzero pixels outside the region of support with zero valued pixels. The Fourier domain constraints involve a Wiener-like filtering operation

$$\tilde{H}_k(u,v) = \frac{G(u,v)\hat{F}^*_{k-1}(u,v)}{|\hat{F}_{k-1}(u,v)|^2 + \ alpha/|\tilde{H}_{k-1}(u,v)|2} \quad (22)$$

$$\tilde{F}_k(u,v) = \frac{G(u,v)\hat{H}^*_{k-1}(u,v)}{|\hat{H}_{k-1}(u,v)|^2 + \alpha/|\tilde{F}_{k-1}(u,v)|^2}. \quad (23)$$

The real constant α represents the energy of the additive noise and is determined by prior knowledge of the noise contamination level, if available. The algorithm is run for a specified number of iterations, which is denoted *MaxIter*, or until the estimates begin to converge. The method is popular for its low computational complexity. The major drawback of the method is its lack of reliability. The uniqueness and convergence properties are, as yet, uncertain. In addition, the restoration is sensitive to the initial image estimate, and the algorithm often exhibits instability.

The conjugate gradient method was proposed by Lane [20] to alleviate the problems associated with the instability of the iterative blind deconvolution method. The image and PSF are assumed to be nonnegative with known finite support. Essentially, the procedure involves the minimization of the following cost function using the conjugate gradient optimization routine:

$$J(\hat{f}(x,y),\hat{h}(x,y)) = \sum_{(x,y)\in\gamma_f} \hat{f}^2(x,y) + \sum_{(x,y)\in\gamma_h} \hat{h}^2(x,y) + \sum_{\forall(u,v)} |G(u,v) - \hat{F}(u,v)\hat{H}(u,v)|^2 \quad (24)$$

where γ_f and γ_h represent pixels for which the image and PSF estimates violate their known constraints. Although the algorithm has reasonably low computational complexity and is fairly robust to noise, it suffers from convergence to incorrect local minima. The cost J is multimodal; therefore, the minimization routine is often trapped in local minima. Our experience with the algorithm showed that for realistic images, it is difficult to achieve proper convergence.

In contrast, the simulated annealing approach by McCallum [21] entails the minimization of the multimodal cost function

$$J(\hat{f}(x,y),\hat{h}(x,y)) = \sum_{\forall(x,y)} [f(x,y)*h(x,y) - g(x,y)]^2. \quad (25)$$

The image and PSF are assumed to be positive with known finite support. Using these constraints on $\hat{f}(x,y)$ and $\hat{h}(x,y)$, a simulated annealing procedure is employed for the minimization of J. In simulated annealing, estimates of the cost function parameters are iteratively varied to globally minimize J. The parameter values are randomly perturbed. If the perturbation reduces J, then it is accepted; if it increases J, then it is accepted with probability p. The probability p is reduced as the number of iterations increases. In the case of infinite precision and infinitely many iterations, the procedure is guaranteed to reach the global minimum of a multimodal cost function. The restoration algorithm is reliable and provides reasonable results in the presence of noise. The major disadvantage is that convergence to the global minimum of the cost function is slow.

A. Convergence of the Algorithms

Lane's conjugate gradient algorithm failed to produce meaningful results for the examples shown in this paper. Three different images were synthetically blurred: two small binary images of text and a larger more complicated grey-scale image of a toy. The PSF's are referred to by their dimensions and are shown in Fig. 4. Figs. 5–8 show the results of the proposed NAS-RIF algorithm [the iterative blind deconvolution (IBD) method] and McCallum's simulated annealing method. The 21×21 PSF is a Gaussian PSF commonly found in x-ray imaging and astronomy, the 23×23 PSF is a Gaussian-like separable PSF, and the 33×33 PSF is a nonseparable, nonsymmetric PSF that attenuates high-frequency components to a greater degree than the other PSF's.

The restored images and percentage mean square errors (MSE) are displayed. The percentage MSE is defined as

$$\text{MSE}(\hat{f}) \triangleq 100 \frac{\sum_{\forall(x,y)} [a\hat{f}(x,y) - f(x,y)]^2}{\sum_{\forall(x,y)} f^2(x,y)}. \quad (26)$$

Because any scaled version of the image estimate is desired, a is chosen such that MSE$(\hat{f})$ is minimized; specifically,

$$a = \frac{\sum_{\forall(x,y)} f(x,y)\hat{f}(x,y)}{\sum_{\forall(x,y)} \hat{f}^2(x,y)}. \quad (27)$$

The proposed NAS-RIF algorithm produced good results and converged for all examples provided in Figs. 5–8. The IBD method also produced comparable results for simple binary images, but convergence was often slower than the NAS-RIF algorithm. The method became unreliable for more complicated grey-scale images; the IBD method failed to converge for the toy image of Fig. 8, even after several thousand iterations. Its major drawback is that convergence is not guaranteed, and instability often results. In addition, no specific termination conditions exist for the method, and the quality of restoration depends on the initial conditions and the noise parameter α, even in noiseless situations.

Lane's conjugate gradient method has definite termination conditions and does not suffer from instabilities like the IBD method. However, it often exhibits convergence to the local minima of its cost function. Experience shows that for moderate to large size images, selection of initial conditions to achieve global convergence is nearly impossible. For the examples presented in this paper, the method failed to converge to a meaningful solution.

McCallum's simulated annealing method produced comparable results to the NAS-RIF and IBD algorithms for small binary images. The major limitation is that its convergence speed is slow, and the computational complexity is impractically high great for larger images.

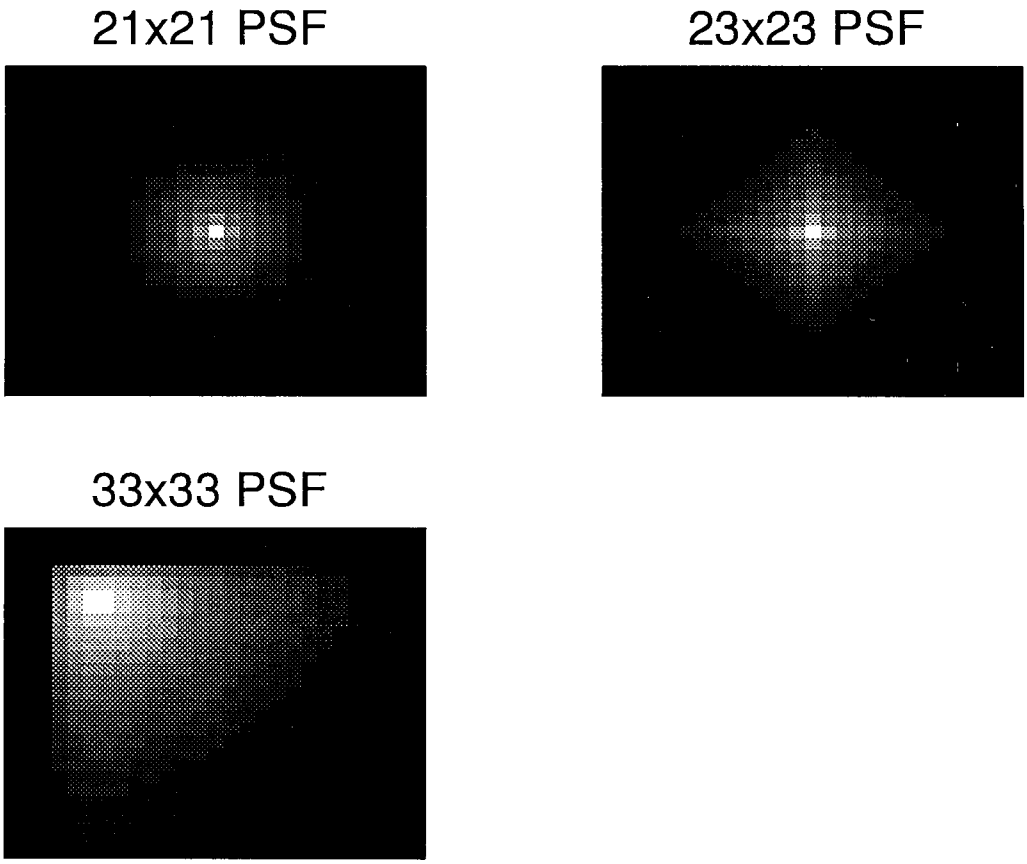

Fig. 4. Synthetic test blurs used for simulations. The blurs are labeled by their dimensions.

TABLE III
COMPUTATIONAL COMPLEXITY OF VARIOUS BLIND DECONVOLUTION ALGORITHMS FOR IMAGES

Algorithm	Total Number of Multiplications for the Example of Figure 5	Order per Iteration
NAS-RIF	4.8×10^7	$N_u N_f N_{ls,k}$
IBD	6.1×10^8	$N_f \log_2(N_f/2)$
McCallum's simulated annealing	1.3×10^{12}	$N_f^2 N_h^2$

B. Computational Complexity

Table III provides a comparison of the computational complexity of the algorithms for the particular example in Fig. 5 and on a per-iteration basis. The second column of Table III gives the total number of multiplications to achieve restoration for the UT blurred image in Fig. 5, and the third column gives the order of the algorithms per iteration. The NAS-RIF algorithm required the fewest multiplications to produce the restored image for the example in Fig. 5. On a *per iteration* basis, the computational complexity of the NAS-RIF algorithm is proportional to the number of FIR filter coefficients $u(x, y)$. In practice, $u(x, y)$ will be moderately sized so that it will not constitute a severe computational burden.

C. Performance Under Nonideal Conditions

Fig. 9 shows the results of the NAS-RIF algorithm for incorrect support size. The restorations of the "BIR" image, of true support 15×65 pixels, blurred by the 21×21 PSF are shown assuming image supports of 17×67 and 13×63. The restoration for overestimation of support size, which is shown in Fig. 9(a), is close to the original image. Underestimation of support size produces poor results. Although the restoration scheme initially seems to converge to the true solution, as shown in the MSE plot of Fig. 9(d), subsequent iterations produce poor results. The other algorithms produce poor results for underestimation of support size as well. McCallum's simulated annealing algorithm is robust to overestimation of the support size, but the IBD method and Lane's conjugate gradient algorithm produce poor results even for an overestimation of support of 10%.

Fig. 10 demonstrates the noise amplification that results in the NAS-RIF method as a function of the number of iterations. Initially, as the number of iterations increases, the image is deblurred, as shown in Fig. 10(c). However, after subsequent iterations, the noise is amplified as demonstrated in Fig. 10(d) and (e). Premature termination is an effective method of regularizing the problem. The IBD method is less susceptible to noise because of the Wiener-like filter that is

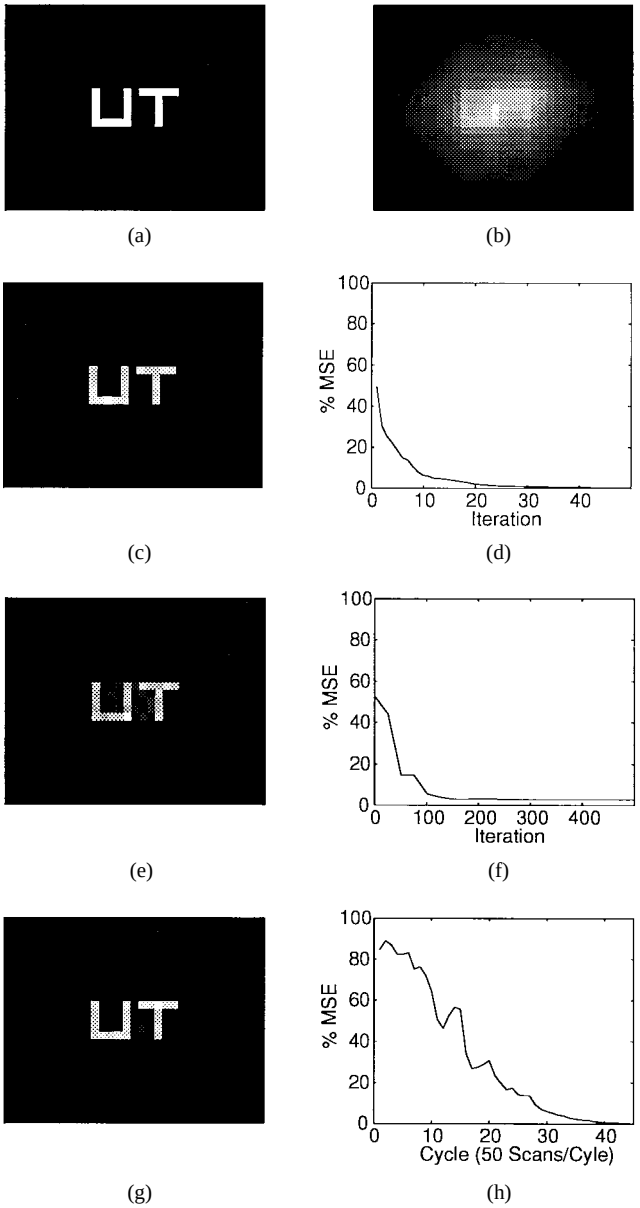

Fig. 5. Results for the UT image degraded by a 23×23 PSF under ideal conditions. (a) Original image. (b) Degraded image using the 23×23 PSF under noiseless conditions. (c), (d) NAS-RIF restoration using $\delta = 0.0138$ and $(N_{xu}, N_{yu}) = (5,5)$. (e), (f) Best IBD restoration using $\alpha = 0.001, MaxIter = 500$. (g), (h) Simulated annealing restoration using $T_0 = J/10$.

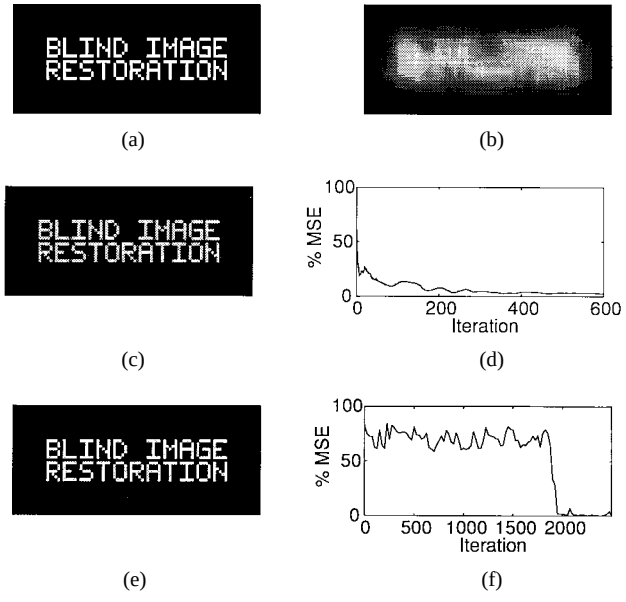

Fig. 6. Results for the BIR image degraded by the 23×23 PSF under ideal conditions. (a) Original image. (b) Degraded image using the 23×23 PSF under noiseless conditions. (c), (d) NAS-RIF restoration using $\delta = 1.00$ and $(N_{xu}, N_{yu}) = (5,5)$. (e), (f) Best IBD restoration using $\alpha = 0.0001, MaxIter = 2500$.

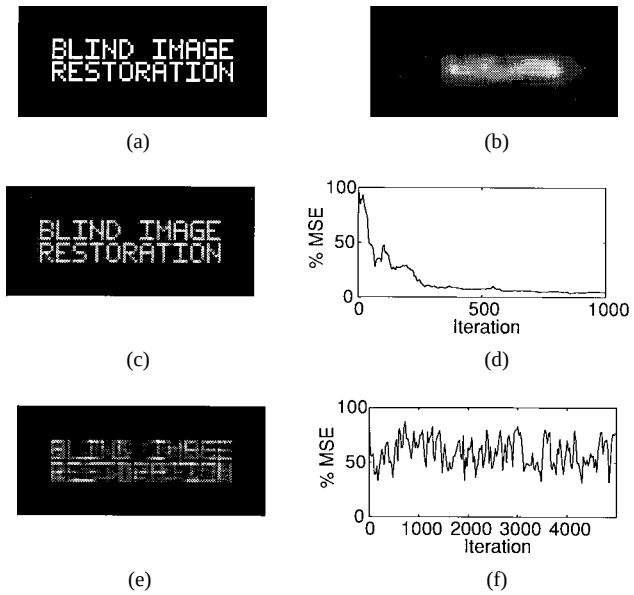

Fig. 7. Results for the BIR image degraded by the 51×51 PSF under ideal conditions. (a) Original image. (b) Degraded image using the 33×33 PSF under noiseless conditions. (c), (d) NAS-RIF restoration using $\delta = 1.20$ and $(N_{xu}, N_{yu}) = (5,5)$. (e), (f) Best IBD restoration using $\alpha = 0.0001, MaxIter = 5000$.

incorporated in the frequency domain. However, it produces poor results as shown in Fig. 10(g) because it fails to converge to a solution for the more complicated grey-scale toy image.

The performance of the NAS-RIF algorithm for real image data is demonstrated in Fig. 11. The real degraded image was prepared by STScI and can be found in their `software/stsdas/testdata/restore/data/jupiter` directory at the `stsci.edu` ftp site. Fig. 11(a) shows the original degraded Hubble data. The NAS-RIF restoration assuming a support of 416×432 after eight iterations is provided in Fig. 11(b). Because of the additive noise present in the data, premature termination based on visual inspection was employed in the NAS-RIF algorithm. Fig. 11(c) shows the normalized (per pixel) cost function for each iteration of the NAS-RIF algorithm. In contrast, the IBD method failed to converge to a solution. Several different random initial estimates were tested, but none converged to a meaningful solution. The results presented here use the blurred image as an initial estimate for the image and a randomly generated image as an initial estimate for the blur. Fig. 11(d) shows the IBD restoration result, which produced the minimum energy deviation from the known nonnegativity and support constraints. This result occurred at the second iteration of the IBD algorithm. This result is visually almost identical

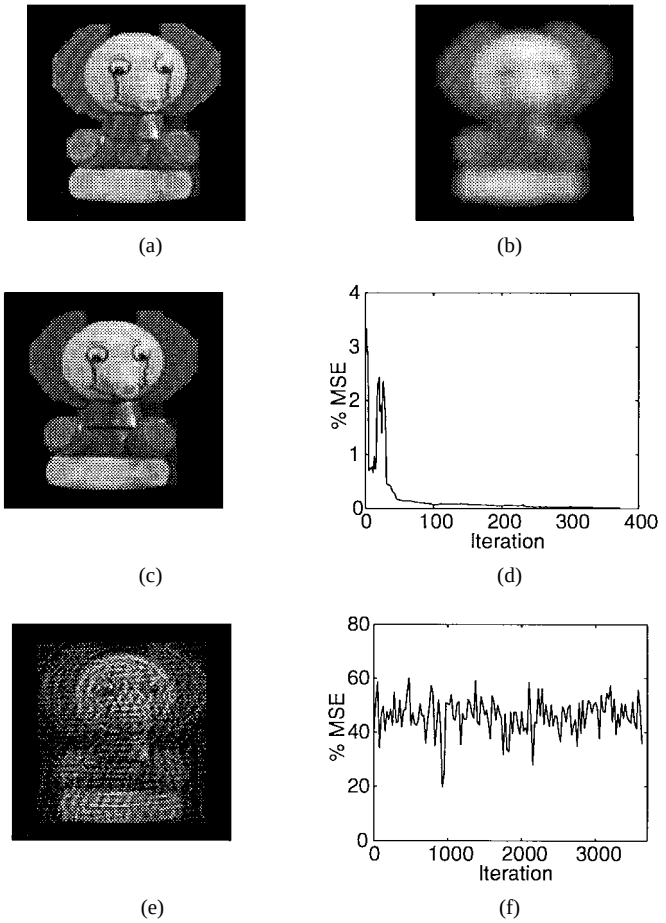

Fig. 8. Results for the toy image degraded by a 21×21 PSF under ideal conditions. (a) Original image. (b) Degraded image using the 21×21 PSF under noiseless conditions. (c), (d) NAS-RIF restoration using $\delta = 0.371$ and $(N_{xu}, N_{yu}) = (5,5)$. (e), (f) Best IBD restoration using $\alpha = 0.0001, MaxIter = 3700$.

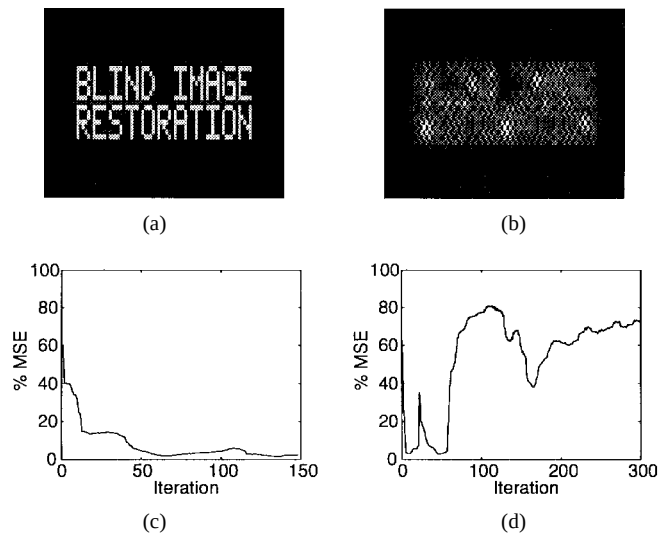

Fig. 9. Results for incorrect estimation of support size for the BIR image (of true support 15×65) degraded by the 21×21 PSF under noiseless conditions. (a), (c) NAS-RIF restoration using $\delta = 1.02$ and $(N_{xu}, N_{yu}) = (5,5)$ (support is overestimated to be 17×67). (b), (d) NAS-RIF restoration using $\delta = 1.02$ and $(N_{xu}, N_{yu}) = (5,5)$ (support is underestimated to be 13×63).

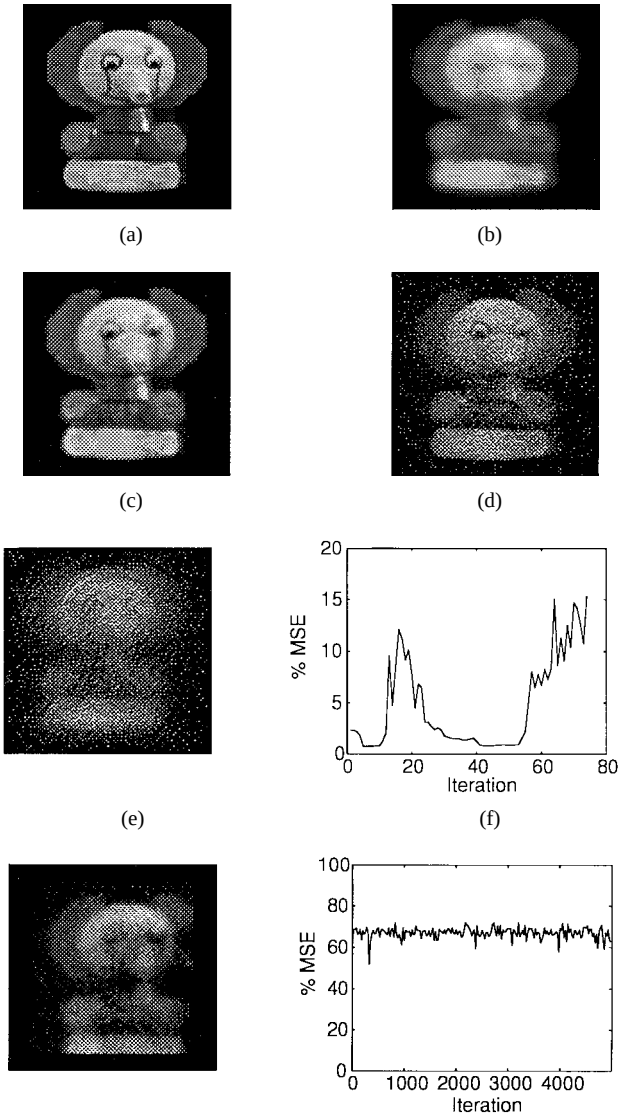

Fig. 10. Results for the toy image degraded by the 21×21 PSF at BSNR of 40 dB. (a) Original image. (b) Degraded image using the 21×21 PSF and a BSNR of 40 dB. (c) NAS-RIF restoration using $(N_{xu}, N_{yu}) = (5,5)$ after nine iterations. (d) NAS-RIF restoration after 23 iterations. (e) NAS-RIF restoration after 74 iterations. (f) MSE plot for NAS-RIF restoration. (g) Best IBD estimate using $\alpha = 0.001, MaxIter = 5000$. (h) MSE for IBD restoration.

to the original blurred image. The normalized (per pixel) energy function for each iteration is shown in Fig. 11(e). In contrast to the NAS-RIF algorithm, the IBD method is not well behaved as the iterations progress. Different values of the noise parameter α were tested, but each one produced the results similar to the one presented.

VII. Conclusions

A novel blind deconvolution scheme for the class of nonparametric finite support restoration methods is developed. It has clear advantages over existing techniques of its class because convergence to the feasible set of solutions is guaranteed. The convexity of the proposed cost function is established analytically. For situations in which the support of the original

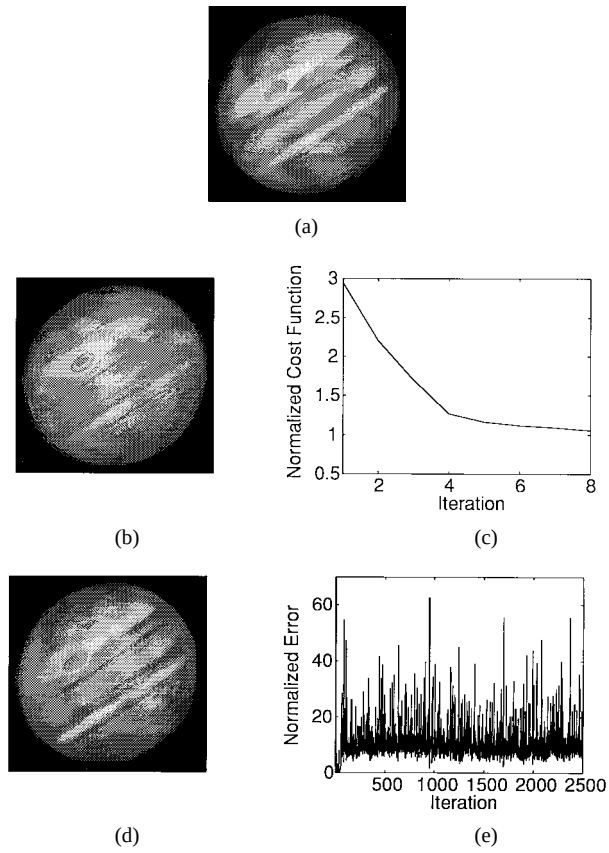

Fig. 11. Results for the Hubble space telescope image of Jupiter. (a) Degraded image. (b) NAS-RIF restoration using $(N_{xu}, N_{yu}) = (31, 31)$ after eight iterations. (c) Normalized cost per iteration for the NAS-RIF restoration. (d) Best IBD estimate using $\alpha = 0.001, MaxIter = 2500$. (e) Error deviation from known constraints per iteration for the IBD method.

image is unknown, a novel support-finding algorithm based on cross validation is presented.

Simulation results of the proposed NAS-RIF method have demonstrated the algorithm's improved speed of convergence over the existing techniques, its superior convergence properties, and its lower computational complexity. Simulations of the blind support-finding algorithm show its potential for blind image restoration applications.

APPENDIX A
PROOF OF CONVEXITY

To prove the convexity of J, the following definition and theorem are used [28].

Definition A.1 (Convex Function): A function J:$\mathbb{R}^N \rightarrow \mathbb{R}$ is said to be convex when, for all $(u, u') \in \mathbb{R}^N \times \mathbb{R}^N$ and all $\alpha \in (0, 1)$, there holds

$$J(\alpha u + (1-\alpha)u') \leq \alpha J(u) + (1-\alpha)J(u'). \tag{28}$$

We denote the class of such functions $Conv\mathbb{R}^N$.

Theorem A.1: Let $J_1, \cdots J_m$ be in $Conv\mathbb{R}^N, t_1, \cdots, t_m$ be positive numbers, and assume that there is a point where all the J_j's are finite. Then, the function

$$J \triangleq \sum_{j=1}^{m} t_j J_j \tag{29}$$

is in $Conv\mathbb{R}^N$.

We break the cost function J into three components, which are denoted J_1, J_2, and J_3. We see from Theorem A.1 that we can prove the convexity of J with respect to u by proving the individual convexities of each component of J. Our analysis first establishes the convexities of J_2 and J_3 and then tackles the more difficult problem of proving the convexity of J_1.

A.1. Proof of Convexity of Support Constraint Cost Function

In this section, we establish the convexity of the component of J resulting from the support constraint on the image estimate. The function is given by

$$J_2 = \sum_{(x,y)\in D_{\text{sup}}} [\hat{f}(x,y) - L_B]^2 \tag{30}$$

where $\hat{f}(x,y) = g(x,y) * u(x,y)$. It is apparent from (30) that J_2 is quadratic with respect to u. It, therefore, follows that J_2 is convex [28].

Similarly, if we consider the component function

$$J_3 = \left[\sum_{\forall(x,y)} u(x,y) - 1\right]^2 \tag{31}$$

we note that J_3 is also quadratic with respect to u and is thus also convex [28].

A.2. Proof of Convexity of the Nonnegativity Constraint Cost Function

In this section, we establish the convexity of the first component of J, which results from the nonnegativity constraint on the image estimate. The function is given by

$$J_1 = \sum_{(x,y)\in D_{\text{sup}}} \hat{f}^2(x,y)\left[\frac{1 - \text{sgn}(\hat{f}(x,y))}{2}\right]. \tag{32}$$

To establish the convexity of J_1, we use the following definition and theorem from [28].

Definition A.2 (Monotone Function): The mapping $\mathcal{J}$:$\mathbb{R}^N \rightarrow \mathbb{R}^N$ is said to be monotone on $\mathbb{R}^N$ when, for all u and u' in $\mathbb{R}^N$

$$\langle \mathcal{J}(u) - \mathcal{J}(u'), u - u' \rangle \geq 0 \tag{33}$$

where $\langle \cdot, \cdot \rangle$ represents the inner product operation

Theorem A.2: Let J be a function differentiable on $\mathbb{R}^N$. Then, J is convex on $\mathbb{R}^N$ if and only if its gradient ∇J is monotone on $\mathbb{R}^N$.

It is easy to see that the derivative of J_1 with respect to $\hat{f}(x,y)$ is given by

$$\begin{aligned}\frac{\partial J_1}{\partial \hat{f}(x,y)} &= 2\hat{f}(x,y)\left[\frac{1 - \text{sgn}(\hat{f}(x,y))}{2}\right] - \frac{\hat{f}^2(x,y)\delta(\hat{f}(x,y))}{2} \\ &= \hat{f}(x,y)[1 - \text{sgn}(\hat{f}(x,y))] \\ &= 2\hat{f}(x,y)u_s(-\hat{f}(x,y))\end{aligned} \tag{34}$$

if $(x,y) \in D_{\text{sup}}$ and is 0 otherwise. The function $\delta(\cdot)$ is the Dirac delta function (distribution), and $u_s(\cdot)$ represents the unit step function, which should not be confused with the FIR

filter $u(x,y)$. The gradient of J_1 with respect to $\{\hat{f}(x,y)\}$ is given by

$$\nabla J_1(\hat{f}) = 2[\hat{f}(1,1)u_s(-f(1,1))\ \hat{f}(1,2)u_s(-f(1,2)) \cdots \hat{f}(N_{xf},N_{yf})u_s(-f(N_{xf},N_{yf}))]^T \quad (35)$$

where $N_{xf} \times N_{yf}$ are the dimensions of the image estimate $\hat{f}(x,y)$. Computing the gradient inner product (GIP)

$$\text{GIP}(\hat{f},\hat{f}') \triangleq \langle \nabla J_1(\hat{f}) - \nabla J_1(\hat{f}'), \hat{f} - \hat{f}' \rangle \quad (36)$$

where $\hat{f}, \hat{f}' \in \mathbb{R}^{N_{xf}N_{yf}}$, we obtain

$$\text{GIP}(\hat{f},\hat{f}') = \sum_{(x,y)\in D_{\text{sup}}} \text{gip}(\hat{f}(x,y),\hat{f}'(x,y)) \quad (37)$$

where

$$\begin{aligned}\text{gip}(\hat{f}(x,y),\hat{f}'(x,y)) &= \hat{f}^2(x,y)u_s(-\hat{f}(x,y)) + \hat{f}'^2(x,y)u_s(-\hat{f}'(x,y)) \\ &\quad - \hat{f}(x,y)\hat{f}'(x,y)[u_s(-\hat{f}(x,y)) + u_s(-\hat{f}'(x,y))].\end{aligned} \quad (38)$$

It is straightforward to see (39), shown at the bottom of the page. It follows from (37) that

$$\langle \nabla J_1(\hat{f}) - \nabla J_1(\hat{f}'), \hat{f} - \hat{f}' \rangle \geq 0. \quad (40)$$

Using Theorem A.2, we see that J_1 is convex with respect to $\hat{f}$. Since $\hat{f}(x,y) = g(x,y) * u(x,y)$, u is related to $\hat{f}$ linearly, J_1 is convex with respect to u [28].

Since J_1, J_2, and J_3 are all convex, it follows from Theorem A.1 that J is convex with respect to its parameters $\{u(1,1),\cdots,u(N_{xu},N_{yu})\}$.

Appendix B
Uniqueness of the Solution

As shown in Appendix A, J can be broken down into three convex component functions J_1, J_2, and J_3. To prove the unimodality of J, it is sufficient to prove the unimodality of any of the component functions. Inspection of the expressions for J_1 and J_3 suggests that neither component is unimodal. For example, assuming that the pixels of the blurred image are nonnegative (which is usually the case for intensity images), any $u(x,y)$ that fulfills the constraints that $\Sigma_{\forall(x,y)}\, u(x,y) = 1$ and $u(x,y) \geq 0$ for all (x,y) globally minimizes J_1 and J_3. Therefore, to find sufficient conditions to ensure the unimodality of J, we find conditions to ensure the unimodality of J_2. We use the following theorem [28]:

Theorem B.1: Let J be twice differentiable on an open convex set $\Omega \subset \mathbb{R}^N$. Then, we have the following.

1) J is convex on Ω if and only if $\nabla^2 J(u_0)$ is positive semidefinite for all $u_0 \in \Omega$.
2) If $\nabla^2 J(u_0)$ is positive definite for all $u_0 \in \Omega$, then J is strictly convex on Ω.

From Theorem B.1, we see that J_2 is unimodal if its Hessian $\nabla^2 J_2$ is positive definite (i.e., $\nabla^2 J_2 > 0$). Since J_2 is convex, it follows from Theorem B.1 that $\nabla^2 J_2$ is positive semidefinite (i.e., $\nabla^2 J_2 \geq 0$).

It is shown in [40] the Hessian matrix of J_2 can be written as

$$\nabla^2 J_2 = 2 \sum_{(x,y)\in \overline{D_{\text{sup}}}} g_{xy} g_{xy}^T \quad (41)$$

where $g_{xy}^T \triangleq [g(x,y)g(x,y-1)\cdots g(x-N_{xu}+1, y-N_{yu}+1)]$. A sufficient condition for $\nabla^2 J_2 > 0$ (i.e., existence of a unique solution) is that there exist $N_{xu}N_{yu}$ linearly independent vectors g_{xy} for $(x,y) \in \overline{D_{\text{sup}}}$ [40].

Appendix C
Effect of Noise on the Global Minimum

This section derives the value of the cost function at the true inverse blur parameter setting for noisy conditions and assuming infinite extent equalizers are available. This value gives an indication of the bias introduced in the restored image. The proposed cost function may be represented as

$$\begin{aligned}J = &\sum_{(x,y)\in D_{\text{sup}}} \hat{f}^2(x,y)\text{cl}(\hat{f}(x,y)) \\ &+ \sum_{(x,y)\in \overline{D_{\text{sup}}}} [\hat{f}(x,y) - L_B]^2 \\ &+ \gamma \left[\sum_{\forall(x,y)} u(x,y) - 1\right]^2\end{aligned} \quad (42)$$

where function $\text{cl}(\cdot)$ is defined as

$$\text{cl}(f) = \frac{1 - \text{sgn}(\hat{f}(x,y))}{2}. \quad (43)$$

The image estimate $\hat{f}(x,y)$ is given by

$$\hat{f}(x,y) = g(x,y) * u(x,y) = \tilde{f}(x,y) + \tilde{n}(x,y) \quad (44)$$

where

$$\begin{aligned}g(x,y) &\triangleq \tilde{g}(x,y) + n(x,y) \\ \tilde{f}(x,y) &\triangleq \tilde{g}(x,y) * u(x,y) \\ \tilde{n}(x,y) &\triangleq n(x,y) * u(x,y)\end{aligned} \quad (45)$$

and $n(x,y)$ is the additive noise.

$$\text{gip}(\hat{f}(x,y),\hat{f}'(x,y)) = \begin{cases} 0 & \text{if } \hat{f}(x,y), \hat{f}'(x,y) \geq 0 \\ \hat{f}^2(x,y) - \hat{f}(x,y)\hat{f}'(x,y) \geq 0 & \text{if } \hat{f}(x,y) \geq 0, \hat{f}'(x,y) < 0 \\ \hat{f}'^2(x,y) - \hat{f}(x,y)\hat{f}'(x,y) \geq 0 & \text{if } \hat{f}(x,y) < 0, \hat{f}'(x,y) \geq 0 \\ (\hat{f}(x,y) - \hat{f}'(x,y))^2 \geq 0 & \text{if } \hat{f}(x,y), \hat{f}'(x,y) < 0 \end{cases} \quad (39)$$

The cost function can be written in terms of $\tilde{f}(x,y)$ and $\tilde{n}(x,y)$ as

$$\begin{aligned} J = & \sum_{(x,y)\in D_{\sup}} [\tilde{f}^2(x,y) + 2\tilde{f}(x,y)\tilde{n}(x,y) + \tilde{n}^2(x,y)] \\ & \cdot [\mathrm{cl}(\tilde{f}(x,y) + \tilde{n}(x,y))] \\ & + \sum_{(x,y)\in \overline{D_{\sup}}} [\tilde{f}^2(x,y) + 2\tilde{f}(x,y)\tilde{n}(x,y) + \tilde{n}^2(x,y) \\ & - 2L_B\tilde{f}(x,y) - 2L_B\tilde{n}(x,y) + L_B^2] \\ & + \gamma\left[\sum_{\forall(x,y)} u(x,y) - 1\right]^2. \end{aligned} \tag{46}$$

Assuming the additive noise is stationary zero-mean and Gaussian, the following expectations are calculated. The term $p_N(n)$ represents the probability density function (pdf) of the noise. Since $n(x,y)$ is zero-mean and Gaussian, $\tilde{n}(x,y)$. which is a filtered version of $n(x,y)$, is also zero-mean and Gaussian with variance

$$\sigma^2 = \sum_{\forall(x_1,y_1)} \sum_{\forall(x_2,y_2)} R_n(x_2 - x_1, y_2 - y_1)u(x_1,y_1)u(x_2,y_2) \tag{47}$$

where $R_n(x,y)$ is the spatial autocorrelation of $n(x,y)$. We find that

$$\begin{aligned} E\{\mathrm{cl}(s+n)\} &= \int_{-\infty}^{\infty} \mathrm{cl}(s+n)p_N(n)\,dn \\ &= \frac{1}{\sqrt{2\pi}\sigma}\int_{-\infty}^{-s} e^{-n^2/2\sigma^2}\,dn \\ &= 1 - Q\left(\frac{-s}{\sqrt{2}\sigma}\right) \end{aligned} \tag{48}$$

$$\begin{aligned} E\{n\mathrm{cl}(s+n)\} &= \int_{-\infty}^{\infty} n\mathrm{cl}(s+n)p_N(n)\,dn \\ &= \frac{-\sigma}{\sqrt{2\pi}} e^{-s^2/2\sigma^2} \end{aligned} \tag{49}$$

$$\begin{aligned} E\{n^2\mathrm{cl}(s+n)\} &= \int_{-\infty}^{\infty} n^2\mathrm{cl}(s+n)p_N(n)\,dn \\ &= \frac{s\sigma}{\sqrt{2\pi}} e^{-s^2/2\sigma^2} + \sigma^2\left[1 - Q\left(\frac{-s}{\sqrt{2}\sigma}\right)\right] \end{aligned} \tag{50}$$

where

$$Q(s) \triangleq \frac{1}{\sqrt{2\pi}}\int_s^{\infty} e^{-\xi^2}\,d\xi. \tag{51}$$

Using these results, the expectation of the cost in the presence of noise at the true inverse PSF u^* is evaluated. It should be noted that $\tilde{f}(x,y) = u^*(x,y) * \tilde{g}(x,y) = f(x,y)$, and $\Sigma_{\forall(x,y)} u^*(x,y) = 1$ if $\gamma \neq 0$ (the situation of a black background).

$$\begin{aligned} E\{J(u^*)\} = & [f^2(x,y) + 2f(x,y)E\{\tilde{n}(x,y)\mathrm{cl}(\tilde{f}(x,y) \\ & + \tilde{n}(x,y))\} + E\{\tilde{n}^2(x,y)\mathrm{cl}(\tilde{f}(x,y) \\ & + \tilde{n}(x,y))] \\ & + \sum_{(x,y)\in\overline{D_{\sup}}} [f^2(x,y) + 2f(x,y)E\{\tilde{n}(x,y)\} \\ & + E\{\tilde{n}^2(x,y)\} \\ & - 2L_Bf(x,y) - 2L_BE\{\tilde{n}(x,y)\} + L_B^2] \\ = & \sum_{(x,y)\in D_{\sup}} \left[(f^2(x,y) + \sigma^2)\right. \\ & \cdot \left(1 - Q\left(\frac{-f(x,y)}{\sqrt{2}\sigma}\right)\right) \\ & \left. - \sigma\frac{f(x,y)}{\sqrt{2\pi}} e^{-f^2(x,y)/2\sigma^2}\right] + \sum_{(x,y)\in\overline{D_{\sup}}} \sigma^2 \end{aligned} \tag{52}$$

because $E\{\tilde{n}(x,y)\} = 0$ and $f(x,y)$ is equal to L_B for $(x,y) \in \overline{D_{\sup}}$.

Therefore, the bias of the cost function due to zero-mean AWGN is given by

$$\begin{aligned} & E\{J(u^*(x,y))\} \\ & \quad = \sum_{(x,y)\in D_{\sup}} (f^2(x,y) + \sigma^2)\left(1 - Q\left(\frac{-f(x,y)}{\sqrt{2}\sigma}\right)\right) \\ & \qquad - \sum_{(x,y)\in D_{\sup}} \sigma\frac{f(x,y)}{\sqrt{2\pi}} e^{-f^2(x,y)/2\sigma^2} + \sigma^2||\overline{D_{\sup}}|| \end{aligned} \tag{53}$$

where $||\overline{D_{\sup}}||$ represents the number of elements in $\overline{D_{\sup}}$. For the case that $n(x,y)$ is zero-mean additive white Gaussian noise (AWGN) with variance σ_n^2

$$\begin{aligned} \sigma^2 &= E\{\tilde{n}^2(x,y)\} = E\{[n(x,y) * u(x,y)]^2\} \\ &= \sigma_n^2 \sum_{x_1=-\infty}^{\infty} \sum_{y_1=-\infty}^{\infty} [u^*(x_1,y_1)]^2. \end{aligned} \tag{54}$$

REFERENCES

[1] A. K. Katsaggelos, Ed., *Digital Image Restoration*. New York: Springer-Verlag, 1991.

[2] R. H. T. Bates, "Astronomical speckle imaging," *Phys. Rep.*, vol. 90, no. 4, pp. 203–297, Oct. 1982.

[3] P. Nisenson and R. Barakat, "Partial atmospheric correction with adaptive optics," *J. Opt. Soc. Amer. A*, vol. 4, pp. 2249–2253, 1991.

[4] D. Kundur and D. Hatzinakos, "Blind image restoration via recursive filtering," in *Proc. IEEE Int. Conf. Acoust., Speech, Signal Processing*, 1996, vol. 4, pp. 2283–2286.

[5] M. Cannon, "Blind deconvolution of spatially invariant image blurs with phase," *IEEE Trans. Acoust., Speech, Signal Processing*, vol. ASSP-24, pp. 58–63, Feb. 1976.

[6] D. C. Ghiglia, L. A. Romero, and G. A. Mastin, "Systematic approach to two-dimensional blind deconvolution by zero-sheet separation," *J. Opt. Soc. Amer. A*, vol. 10, no. 5, pp. 1024–1036, May 1993.

[7] R. L. Lagendijk, A. M. Tekalp, and J. Biemond, "Maximum likelihood image and blur identification: A unifying approach," *Opt. Eng.*, vol. 29, no. 5, pp. 422–435, May 1990.

[8] R. L. Lagendijk, J. Biemond, and D. E. Boekee, "Identification and restoration of noisy blurred images using the expectation-maximization algorithm," *IEEE Trans. Acoust., Speech, Signal Processing*, vol. 38, July 1990.

[9] A. K. Katsaggelos and K.-T. Lay, "Image identification and image restoration based on the expectation-maximization algorithm," *Opt. Eng.*, vol. 29, no. 5, pp. 436–445, May 1990.

[10] B. C. Tom, K.-T. Lay, and A. K. Katsaggelos, "Multichannel image identification and restoration using the expectation-maximization algorithm," *Opt. Eng.*, vol. 35, no. 1, pp. 241–254, Jan. 1996.

[11] T. J. Holmes *et al.*, "Light microscopic images reconstructed by maximum likelihood deconvolution," in *Handbook of Biological and Confocal Microscopy*, 2nd ed., J. B. Pawley, Ed. New York: Plenum, 1995.
[12] T. J. Holmes, "Blind deconvolution of quantum-limited incoherent imagery: maximum-likelihood approach," *J. Opt. Soc. Amer. A.*, vol. 9, no. 7, July 1992.
[13] V. Krishnamurthi, Y.-H. Liu, S. Bhattacharyya, J. N. Turner, and T. J. Holmes, "Blind deconvolution of fluorescence micrographs by maximum- likelihood estimation," *Applied Opt.*, vol. 34, no. 29, pp. 6633–6647, Oct. 1995.
[14] S. J. Reeves and R. M. Mersereau, "Blur identification by the method of generalized cross-validation," *IEEE Trans. Image Processing*, vol. 1, pp. 301–311, July 1992.
[15] G. Jacovitti and A. Neri, "A Bayesian approach to 2D non minimum phase AR identification," in *Proc. Fifth AASP Workshop Spectrum Estimation Modeling*, 1990, pp. 79–83.
[16] A. P. Petropulu and C. L. Nikias, "Blind deconvolution using signal reconstruction from partial higher order cepstral information," *IEEE Trans. Signal Processing*, vol. 41, pp. 2088–2095, June 1993.
[17] ——, "Blind deconvolution based on signal reconstruction from partial information using higher-order spectra," in *Proc. Int. Conf. Acoust., Speech Signal Process.*, 1991, vol. 30, pp. 1757–1760.
[18] G. R. Ayers and J. C. Dainty, "Iterative blind deconvolution method and its applications," *Opt. Lett.*, vol. 13, no. 7, pp. 547–549, July 1988.
[19] B. L. K. Davey, R. G. Lane, and R. H. T. Bates, "Blind deconvolution of noisy complex-valued image," *Opt. Commun.*, vol. 69, nos. 5 and 6, pp. 353–356, Jan. 1989.
[20] R. G. Lane, "Blind deconvolution of speckle images," *J. Opt. Soc. Amer. A.*, vol. 9, no. 9, pp. 1508–1514, Sept. 1992.
[21] B. C. McCallum, "Blind deconvolution by simulated annealing," *Opt. Commun.*, vol. 75, no. 2, pp. 101–105, Feb. 1990.
[22] Y. Yang, N. P. Galatsanos, and H. Stark, "Projection-based blind deconvolution," *J. Opt. Soc. Amer. A*, vol. 11, no. 9, pp. 2401–2409, Sept. 1994.
[23] D. Kundur and D. Hatzinakos, "Blind image deconvolution," *IEEE Signal Processing Mag.*, vol. 13, pp. 43–64, May 1996.
[24] R. M. Mersereau and R. W. Schafer, "Comparative study of iterative deconvolution algorithms," in *Proc. IEEE Int. Conf. Acoust., Speech, Signal Process.*, Apr. 1978, pp. 192–195.
[25] R. W. Schafer, R. M. Mersereau, and M. A. Richards, "Constrained iterative signal restoration algorithms," *Proc. IEEE*, vol. 69, pp. 432–450, Apr. 1981.
[26] R. Marucii, R. M. Mersereau, and R. W. Schafer, "Constrained iterative deconvolution using a conjugate gradient algorithm," in *Proc. IEEE Int. Conf. Acoust., Speech, Signal Process.*, 1982, pp. 1845–1848.
[27] R. Prost and R. Goutte, "Discrete constrained iterative deconvolution with optimized rate of convergence," *Signal Process.*, vol. 7, pp. 209–230, Dec. 1984.
[28] J. B. Hiriart-Urruty and C. Lemarécal, *Convex Analysis and Minimization Algorithms I.* New York: Springer-Verlag, 1993.
[29] M. E. Zervakis and A. N. Venetsenopoulos, "Resolution-to-noise tradeoff in linear image restoration," *IEEE Trans. Circuits Syst.*, vol. 38, pp. 1206-1212, Oct. 1991.
[30] D. Kundur, "Blind deconvolution of still images using recursive inverse filtering," M.A.Sc. thesis, Univ. Toronto, Toronto, Ont., Canada, 1995.
[31] D. L. Snyder, L. J. Thomas, Jr., and D. G. Politte, "Noise and edge artifacts in maximum-likelihood reconstruction for emission tomography," *IEEE Trans. Med. Imag.*, vol. ME-6, pp. 228–237, May 1987.
[32] J. Biemond, R. L. Lagendijk, and R. M. Mersereau, "Iterative methods for image deblurring," *Proc. IEEE*, vol. 78, pp. 856–883, May 1990.
[33] H. J. Trussell, "Convergence criteria for iterative restoration methods," *IEEE Trans. Acoust., Speech, Signal Processing*, vol. ASSP-31, pp. 201–212, Feb. 1983.
[34] B. J. Sullivan and A. K. Katsaggelos, "New termination rule for linear iterative image restoration algorithms," *Opt. Eng.*, vol. 29, no. 5, pp. 471–477, May 1990.
[35] B. J. Sullivan and H. C. Chang, "A general landweber iteration for ill-conditioned signal restoration," in *Proc. IEEE Int. Conf. Acoust., Speech, Signal Process.*, 1991, pp. 1729–1732.
[36] S. J. Reeves and K. M. Perry, "A practical stopping rule the iterative image restoration," *Proc. SPIE Image Process. Algorithms Techniques III*, vol. 1657, pp. 192–200, 1992.
[37] S. J. Reeves and M. Mersereau, "Automatic Assessment of constraint sets in image restoration," *IEEE Trans. Image Processing*, vol. 1, pp. 119–123, Jan. 1992.
[38] C. T. Chen, *Linear System Theory and Design.* Toronto, Ont., Canada: Harcourt Brace Jovanovich, 1984, p. 413.
[39] W. H. Press, S. A. Toukolsky, W. T. Vetterling, and B. P. Flannery, *Numerical Recipes in C, The Art of Scientific Computing*, 2nd ed. New York: Cambridge Univ. Press, 1992.
[40] D. Kundur and D. Hatzinakos, "On the global asymptotic convergence of the NAS-RIF algorithm for blind image restoration," in *Proc. IEEE Int. Conf. Image Process.*, Lausanne, Switzerland, Sept. 1996, vol. 3, pp. 73–76.

Deepa Kundur (S'93) was born in Toronto, Ont., Canada. She received the Bachelor of Applied Science degree in 1993 and the Master of Applied Science degree in communications in 1995, both from the Department of Electrical and Computer Engineering, University of Toronto. She is currently pursuing doctoral studies at the University of Toronto.

Her research interests include digital watermarking of multimedia, blind image restoration, and data fusion for the classification of remote sensing imagery. She is currently an engineer in training with the Professional Engineers of Ontario (PEO).

Dimitrios Hatzinakos (M'90) received the Diploma degree from the University of Thessaloniki, Thessaloniki, Greece, in 1983, the M.A.Sc. degree from the University of Ottawa, Ottawa, Ont., Canada, in 1986, and the Ph.D. degree from Northeastern University, Boston, MA, in 1990, all in electrical engineering.

From January 1990 until August 1990 he was a Visiting Assistant Professor at the Department of Electrical and Computer Engineering, Northeastern University. From September 1990 until June 1995, he was an Assistant Professor at the Department of Electrical and Computer Engineering, University of Toronto, Toronto, Ont., Canada, where he now holds the rank of Associate Professor with tenure. His research interests span the fields of digital signal and image processing with applications, higher order spectral analysis, blind and adaptive filter algorithms, and digital communications. He has organized and taught many short courses in signal processing devoted to continuing engineering education and given numerous seminars in the areas of higher order spectra and blind deconvolution. He is author/co-author of more than 60 papers in technical journals and conference proceedings, and he has contributed to four books in his area of interest. His industrial and consulting experience includes consulting through Electrical Engineering Consociates Ltd. Consulting work included contracts with United Signals and Systems, Inc., Burns and Fry, Ltd., Pipetronix, Ltd. and the Defense Research Establishment Ottawa (DREO).

Dr. Hatzinakos served as a member of the conference board of the IEEE Statistical Signal and Array Processing Committee (SSAP) from 1992 until 1995 and Co-Technical Program Chair of the Fifth Workshop on Higher Order Statistics, Banff, Alta., Canada, in July 1997. He is a member of EURASIP, the Professional Engineers of Ontario (PEO), and the Technical Chamber of Greece.